Infrared Absorption Cross-Section Measurements for Nitrous Acid (HONO) at Room Temperature

William S. Barney,[†] Lisa M. Wingen, Matthew J. Lakin, Theo Brauers,[‡] Jochen Stutz,[§] and Barbara J. Finlayson-Pitts*

Department of Chemistry, University of California, Irvine, Irvine, California 92697-2025

Received: August 26, 1999; In Final Form: December 14, 1999

Infrared absorption cross sections for nitrous acid (HONO) were measured using HONO spectra recorded simultaneously by UV/visible and FTIR spectroscopy. HONO was prepared by the reaction of HCl(g) and $NaNO_2$(s) and was introduced into a 561 L environmental chamber equipped with parallel sets of White optics with total path 52.5 m for UV/visible and FTIR spectroscopy. Alternatively, HONO was prepared in situ by reaction of ClNO(g) with water vapor. Absolute concentrations of HONO were determined independently using the UV spectrum and published UV absorption cross sections. All experiments were carried out at 750 Torr total pressure in N_2 at 294−297 K. We report both Q-branch intensities and integrated absorbances for the HONO modes trans-ν_3 (1263 cm^{-1}), cis-ν_4 (852 cm^{-1}), and trans-ν_4 (790 cm^{-1}). For trans-ν_3 and cis-ν_4 we also include synthetic reference spectra composed of Gaussian functions which give an accurate reproduction of our experimental references, and can easily be generated by computer for ease of use in other laboratories.

Introduction

Photolysis of nitrous acid (HONO) is an important source of the OH radical in the polluted troposphere. For example, Winer and Biermann[1] reported that HONO photolysis accounted for almost all the OH produced during the first few hours after sunrise on a typical day in Long Beach, CA. OH is a key reactive species in the troposphere, initiating the oxidation of CO and SO_2 as well as volatile organic compounds (VOCs). A byproduct of VOC oxidation is the catalytic oxidation of NO to NO_2, which is the only known anthropogenic source of tropospheric ozone.[2] In addition to being a source of OH, HONO has been shown to form nitrous oxide[3,4] in a surface reaction whose mechanism is not yet well-defined. This is potentially significant on a global scale, since there are uncertainties in the budget[5,6] of N_2O.

In polluted areas, HONO accumulates at night, with concentrations occasionally as high as 10 ppb, depending on local chemistry and meteorology.[7] HONO is formed by heterogeneous chemistry of NO_2 in the presence of water on the surfaces of reaction chambers[7−17] and indoor environments.[18−20] HONO has also been observed from reactions of NO_2 on soot.[21−24] However, the specific mechanisms by which these reactions proceed are still elusive, and are the subject of continuing laboratory studies.

HONO is often measured in laboratory studies by UV/visible differential optical absorption spectroscopy (DOAS) or by Fourier transform infrared spectroscopy (FTIR). DOAS[25] is a sensitive and specific technique that makes use of differential, rather than absolute, absorption cross sections. Ultraviolet absorptions may consist of both broad and structured components, and DOAS employs nonlinear least-squares analysis to separate the structured part of the spectrum from the broad part, which may contain contributions from unknown or unidentified species. DOAS has better sensitivity to HONO than IR, primarily because the detector noise is lower, and because other common atmospheric species such as water vapor do not interfere. However, in laboratory studies, ppb sensitivity is often not required, and FTIR has the advantage that it can be used to simultaneously measure many species such as HCl, ClNO, HNO_3, and N_2O. These species cannot be detected by DOAS because they do not have a structured UV absorption spectrum. A number of laboratories[12,26−32] have chosen FTIR in addition to, or instead of, DOAS as a HONO measurement technique.

Despite the widespread use of FTIR to measure HONO, there have been relatively few measurements of the HONO IR absorption cross sections. The absolute cross sections available in the literature include those of Chan et al.[29] and of Sakamaki et al.[8] Kagann and Maki[30] published integrated cross sections of 10 absorption bands, including spectra of the bands at 3590, 1699, 1640, and 1263 cm^{-1}. Wallington and Japar[27] have used unpublished cross sections measured in their lab. Tunable diode laser spectroscopy (TDLS) line intensity measurements have been made by Maki,[33] and, using very high-purity (NO_2-free) HONO, by Becker et al.[34]

HONO exists in equilibrium with NO_2, H_2O, and other compounds such as NO or HNO_3, so samples with 100% purity cannot be prepared. Febo and co-workers[35] have prepared samples that contain very low levels of most impurities, but even these are not entirely free of NO_2. As a result, a major challenge in measuring the HONO cross section is determining the amount of nitrous acid present in the gas mixture. This is probably at least a partial source of the discrepancies, on the order of 30−40%, in the cross sections reported in various studies.[8,29] A second challenge in measuring IR cross sections

* To whom correspondence should be addressed. E-mail: BJFINLAY@UCI.EDU. Phone: (949) 824−7670. Fax: (949) 824−3168.

[†] Current address: Department of Environmental Engineering Science, California Institute of Technology, Pasadena, CA 91125.

[‡] Institut für Atmosphärische Chemie (ICG-3), Forschungszentrum Jülich, 52425 Jülich, Germany.

[§] Department of Atmospheric Sciences, University of California, Los Angeles, Los Angeles, CA 90024-1565.

10.1021/jp9930503 CCC: $19.00
Published on Web 02/05/2000

TABLE 1: Experimental Conditions[a]

expt	method of HONO synthesis[b]	$[HONO]_{max}$ (10^{13} molecules cm^{-3})	$[NO_2]_{max}$ (10^{13} molecules cm^{-3})	$[HNO_3]_{max}$ (10^{13} molecules cm^{-3})	$[H_2O]_{max}$ (10^{16} molecules cm^{-3})	10^{-11} a_ν[c] 1263	852	790
2	$NaNO_2$ + HCl	7.2	13.	0.4	14.	242	1.68	1.94
3	$NaNO_2$ + HCl	8.4	14.	1.0	14.	243	1.70	1.94
4	ClNO + H_2O	1.5	0.18	<0.1	14.	226	1.70	*d*, *e*
5	ClNO + H_2O	1.2	0.16	<0.1	7.0	231	1.73	*e*
6	$NaNO_2$ + HCl	2.9	1.9	0.4	7.0	229	1.72	1.92
7	$NaNO_2$ + HCl	2.5	1.9	0.4	4.0	245	*e*	2.02
8	$NaNO_2$ + HCl	4.1	1.9	0.4	3.0	234	1.71	2.02
9	$NaNO_2$ + HCl	4.0	2.0	0.2	3.0	233	1.66	1.90

[a] All experiments were done in ~750 Torr of N_2 and 21−24 °C. Details are given in the Experimental Section and by Wingen et al.[32] Experiment no. 1 was not used in the present analysis so is omitted here. [b] $NaNO_2$ + HCl: this reaction was used to generate gaseous HONO, which was flowed into the chamber. ClNO + H_2O: gaseous ClNO and H_2O were introduced into the chamber and HONO production from the reverse of reaction 1 was followed with time. See text for details. [c] The concentration associated with reference ν, from eq VI. Reference spectra were initially scaled differently, so a_ν does not have the same order of magnitude for each absorption band. *y*-intercepts were fixed to zero except where noted. [d] The HONO 790 cm^{-1} band did not give reliable results for this experiment due to large changes in the baseline over time. [e] *y*-intercept was floated in order to get an acceptable fit.

is that many likely impurities, including water, HNO_3, NO_2, NO, N_2O_4, N_2O, and others, may overlap the HONO bands.

We report here FTIR absorption cross sections for HONO determined for the first time by simultaneous FTIR and DOAS measurements, using the revised UV/visible cross sections of Bongartz et al.[36,37] This approach avoids the problem of indirectly determining the HONO concentration. In the event of future revisions to the UV cross sections, the FTIR cross sections reported here can easily be rescaled accordingly.

Experimental Section

Experiments were conducted in a 561 L environmental chamber. The chamber is described fully elsewhere,[38] so only a brief description will be given here. It is rectangular, 48 × 48 × 220 cm, consisting of an aluminum baseplate and stainless steel frame with 17 removable panels (41 × 41 cm) made of aluminum. The surface-to-volume ratio is 0.08 cm^{-1}. With the exception of windows and mirrors, the inner surfaces of the chamber are coated with halocarbon wax (Halocarbon Products Corp., Series 1500) to minimize surface reactivity. Pressure measurements are made with a Leybold CMH1000 capacitance manometer accurate to ±0.25% (at atmospheric pressure) and a Vaisala HMP234 temperature/humidity gauge accurate to ±0.1 °C and ±2% RH. The chamber can be evacuated to $<10^{-3}$ Torr using a mechanical pump and two sorption pumps.

The IR system (Mattson Infinity AR), with its entire external optical path and HgCdTe detector, is enclosed in a Plexiglas box that is purged with dry nitrogen during the experiments. IR spectra consisted of 32 coadded scans at 0.5 cm^{-1} resolution. The IR beam enters and exits the chamber through 1° wedge ZnSe windows, which are resistant to water and somewhat resistant to nitrogen oxides. A set of gold-coated White optics[39] (base path length 200 cm) allow multiple passes through the chamber. In this work, 26 passes were used, increasing the path length to 5253 ± 7 cm.

The DOAS light source is a high-pressure xenon arc lamp (Oriel). A quartz entrance/exit window is used. A second set of White cell optics is used for the UV beam. These are installed parallel to the IR optics and have a protected aluminum coating, but are otherwise identical to the IR optics. The light exiting from the chamber is focused on the entrance slit of a Jobin Yvon-Spex (model 460MST24) monochromator equipped with a holographic grating (1200 grooves/mm blazed at 330 nm) and a 1024-channel diode array detector. The dispersion of 0.0433 ± 0.0002 nm/pixel gives a spectral range of approximately 44 nm. HONO/NO_2 bands were monitored in the 340−380 nm region with a resolution of 0.27 nm. Absolute wavelength calibration is maintained by recording a mercury lamp spectrum at the beginning of each experiment.

HONO was produced by the reaction of HCl(g) with $NaNO_2$(s) using a modification[32] of the method of Febo et al.[35] Nitrogen gas (Oxygen Service Co., 99.999%) was flowed over a solution of 5.2 M HCl (prepared from Fisher HCl, 12.1 M) held at 0 °C with an ice bath. The HCl/H_2O/N_2 gas mixture flowed upward through a glass frit which supported about 20 g of $NaNO_2$ powder (Fisher, 99.6%). In some experiments it was necessary to add about 2 mL of Nanopure H_2O (Barnstead, 18.2 MΩ·cm) dropwise to the $NaNO_2$ prior to starting the flow of gas. This prevented large quantities of unreacted HCl from passing through the $NaNO_2$ and destroying the HONO product.[32] In other experiments, "super free-flowing" grade $NaNO_2$ was used, described by the manufacturer as being sieved to remove clumps (Aldrich, 99.5%). This allowed low-humidity spectra to be recorded, although some HCl did enter the product stream, limiting the amount of HONO that could be produced to about 1.5 ppm for these experiments. The free-flowing $NaNO_2$ allowed lower N_2 flow rates to be used, which greatly decreased the amount of NO_2 impurity. HONO was introduced into the chamber as it was produced, and the chamber was filled until the relative humidity was between 10 and 30%.

In order to study a range of concentrations, six experiments were carried out in which an initial concentration of HONO was reacted with an excess of gaseous HCl:

$$HCl + HONO \rightarrow ClNO + H_2O \qquad (1)$$

This slow[32] reaction proceeded over a period of hours, producing a range of HONO concentrations. Two other experiments used the reverse of (1) to produce HONO *in situ*. In these experiments, ClNO was prepared[32] by condensing Cl_2 (Matheson, 99.5%) and an excess of NO (Matheson, 99%) into a trap at 77 K and then warming to room temperature. Unreacted NO was pumped off using a trap held at 196 K by a CO_2/acetone bath. ClNO was added to the chamber, which was subsequently filled with 750 Torr of N_2 at a controlled humidity. Initial HONO concentrations varied between 0.5 and 3.5 ppm; NO_2 impurities between 0.07 and 5.7 ppm. All spectra were taken at approximately 750 Torr total pressure in N_2. All pressure measurements were accurate to ±0.1%, and volume measurements to ±0.3%. The conditions for each experiment are summarized in Table 1.

Reference Spectra. Concentrations for HNO_3, NO_2, and H_2O were determined by fitting a reference spectrum of the pure gas (recorded in our chamber) to the experimental spectrum. The reference sample was repeatedly diluted, producing a set of six or seven calibration points at different concentrations for each gas. NO_2 was synthesized by combining an excess of O_2 (Oxygen Service Co., 99.993%) with NO which had been passed through a trap at 196 K to remove impurities such as HNO_3; the excess O_2 was removed by pumping through a CO_2/acetone bath, which retained the NO_2. Measured NO_2 pressures were corrected for N_2O_4 using the equilibrium constant[40] $[N_2O_4]/[NO_2]^2 = 2.5 \times 10^{-19}$ cm^3 molecule^{-1}. The dry HNO_3 sample was prepared from the vapor above a 2:1 mixture of H_2SO_4:HNO_3 (H_2SO_4, Fisher, 18 M; HNO_3, Fisher, 15.8 M). Our infrared spectra give an average cross section (0.5 cm^{-1} resolution, base 10) of $(5.1\pm 0.9, 2\sigma) \times 10^{-20}$ cm^2 molecule^{-1} for the NO_2 band at 2920 cm^{-1}, in good agreement with the value of Sakamaki et al.[8] of 4.67×10^{-20} cm^2 molecule^{-1}. Our HNO_3 calibration gives an integrated (base 10) cross section of $(8.48 \pm 0.34, 2\sigma) \times 10^{-17}$ cm molecule^{-1} over the range 840−930 cm^{-1}, in good agreement with the value 8.13×10^{-17} cm molecule^{-1} obtained for the same range by Hjorth et al.[41] The high water concentrations present (2000−6000 ppm) meant that water absorptions were not linear with respect to concentration, so the reference spectrum used for analysis was chosen to be as close as possible to the actual concentration used in the experiment. The water reference spectra were obtained from mixtures of dry and humidified UHP N_2.

Data Analysis

Spectroscopic Analysis. Spectral analysis was done using the program MFC.[42] The details of the analysis are described elsewhere,[43,44] so only a short summary will be given here. In a gas mixture with m absorbers, the intensity $I(\lambda)$ at the detector may be written

$$I(\lambda) = I_0(\lambda) \exp[-R(\lambda) - l\sum_{j=1}^{m}\sigma(\lambda)_j C_j] \qquad \text{(I)}$$

Here $I_0(\lambda)$ is the source intensity transmitted through an empty chamber, and l is the path length. $R(\lambda)$ represents other changes in the background intensity not due to absorption, including scattering and time variation of the detector sensitivity. C_j and σ_j are the concentration and absorption cross section, respectively, of the jth absorber. We further make the simplifying assumption that $\sigma(\lambda)$ can be split into a structured part, $\sigma_S(\lambda)$, and a broad, structureless part, $\sigma_B(\lambda)$. Taking the logarithm of (I), and showing the contributions of the structured and broad absorptions separately, one obtains

$$\ln \frac{I(\lambda)}{I_0(\lambda)} = -R(\lambda) - l\sum_{j=1}^{m} C_j\sigma_{Bj}(\lambda) - l\sum_{j=1}^{m} C_j\sigma_{Sj}(\lambda) \qquad \text{(II)}$$

The broad component of the absorption can be simplified to a single function of wavelength

$$B(\lambda) = l\sum_{j=1}^{m} C_j\sigma_{Bj}(\lambda) \qquad \text{(III)}$$

giving

$$\ln\frac{I_0(\lambda)}{I(\lambda)} = R(\lambda) + B(\lambda) + l\sum_{j=1}^{m} C_j\sigma_{Sj}(\lambda) \qquad \text{(IV)}$$

$R(\lambda)$ and $B(\lambda)$ are both broad and can be described by a low-order polynomial in λ. If the structured absorption $\sigma_{Sj}(\lambda)$ of the jth individual absorber can be fit by an independent reference spectrum $S_j(\lambda)$, then the concentration C_j can be determined by a linear least-squares using the model function $F(\lambda)$ to fit the observed spectrum:

$$F(\lambda) = P(\lambda) + l\sum_{j=1}^{m} c_j S_j(\lambda) \qquad \text{(V)}$$

Here c_j are the scaling parameters for the reference spectra $S_j(\lambda)$ which give the best fit to the observed spectrum. The c_j are proportional to the true concentrations C_j. $P(\lambda)$ is a polynomial of sufficiently high order that it will fit the broad part of the absorption spectrum very well, but not so high as to reproduce structured absorptions. For the work described in this paper, polynomials of order 0−3 were typically used. The polynomial is not strictly independent of the concentrations C_j because $B(\lambda)$ in expression III depends on C_j, and the scattering terms in $R(\lambda)$ may also depend on C_j. However, our analysis depends on correctly measuring the structured (differential) part of the absorption only, and no physical significance is given to the polynomial.

In the above discussion, we have neglected the effects of using a discrete diode array; however, these effects were included in our analysis for the UV spectra. In particular, we used a "shift and squeeze" method to compensate for the possibility that the grating position or dispersion might change slightly between experiments. For a complete discussion, see Stutz and Platt.[44]

UV and IR HONO references $S^{UV,IR}_{HONO}(\lambda)$ were created from spectra of the experiments summarized in Table 1. In the IR, interfering absorbances were subtracted, where necessary. The amount of a reference to be subtracted was determined by fitting the reference to the experimental spectrum in a nearby region that contained no HONO absorption. While less direct, this is the only method of subtraction that could be used, given that no authentic HONO spectrum was available. In the case of water where relative intensities of the bands in the subtraction region and the nearby fitting region may differ greatly, we used only water spectra that represented the same approximate concentration present in the experiment. $S^{UV}_{HONO}(\lambda)$ was determined from a single UV reference spectrum, while averaging was used to correct for possible subtraction errors in the IR spectra. Eight selected HONO spectra, one from each experiment, were averaged to create the three $S^{IR}_{HONO}(\lambda)$ (ν = 1263, 852, or 790 cm^{-1}). $S^{UV}_{HONO}(\lambda)$ was calibrated by fitting it to the published spectrum of Bongartz et al.[36,37] The literature spectrum was convoluted with our instrument line shape to produce a spectrum $S^{LIT}_{HONO}(\lambda)$ with the correct resolution (0.27 nm) to match our experimental spectra. Fitting our reference $S^{UV}_{HONO}(\lambda)$ to the convoluted literature spectrum $S^{LIT}_{HONO}(\lambda)$ gave the absolute HONO concentration for $S^{UV}_{HONO}(\lambda)$. Figure 1 shows the DOAS reference spectrum $S^{UV}_{HONO}(\lambda)$ compared to the literature reference[36,37] $S^{LIT}_{HONO}(\lambda)$ and to a reference spectrum of NO_2. The differential optical absorption cross sections of our reference NO_2 spectrum are in excellent agreement with the literature.[45]

In all experiments, UV and IR spectra were recorded simultaneously. The HONO concentration $C_{HONO}(t)$ was determined by fitting $S^{UV}_{HONO}(\lambda)$ to the experimental spectrum corresponding to time t. The IR spectra were fit according to eq V using the uncalibrated references for the three different absorption bands $S^{IR}_{HONO}(\lambda)$, producing three time profiles $c_{HONO,\nu}(t)$, where $c_{HONO,\nu}$ are scaling parameters for the HONO references and ν is either 1263, 852, or 790 cm^{-1}.

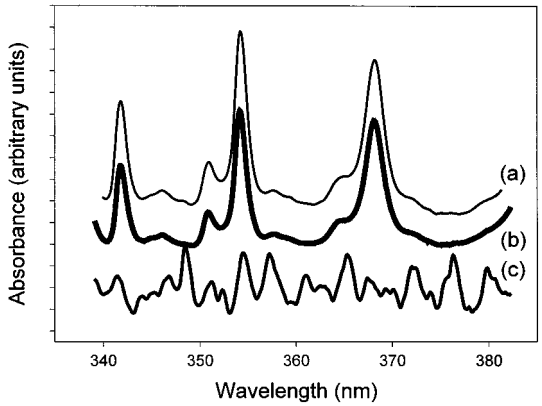

Figure 1. DOAS (UV) spectra of HONO and NO_2: (a) spectrum of HONO from refs 36 and 37; (b) HONO reference spectrum used in this work; (c) NO_2 reference spectrum used in this work. Comparing (b) to (c) shows that there is no significant contribution of NO_2 to our HONO reference spectrum (b).

For each experiment, then, an absolute concentration−time profile $C_{HONO}(t)$ and three relative absorbance−time profiles were obtained. The constant of proportionality, a_ν, could then be determined by a weighted linear regression for the best fit to the equation

$$C_{HONO}(t) = a_\nu c_{HONO,\nu}(t) \qquad \text{(VI)}$$

where $C_{HONO}(t)$ is obtained by DOAS and the *y*-intercept is specified to be zero. From eq V, $c_{HONO,\nu(t)}$ is a unitless coefficient so that a_ν has units of concentration and gives the concentration of HONO. If the *y*-intercept is floated, nonzero values result; however, these are small (less than our detection limit) and fluctuate around zero, thus not indicating a systematic offset in one direction. Figure 2 shows the results of the regression (VI) for a typical experiment, no. 6. These are similar to Beer−Lambert law plots, although the axes are reversed from the usual orientation and the *x*-axis is in relative, not absolute, absorbance units. As can be seen from Table 1, the values of a_ν vary by less than 5% between experiments. The absorption cross sections can then be easily determined:

$$\sigma^{IR}_{HONO}(\lambda) = \frac{S^{IR}_{HONO,\nu}(\lambda)}{a_\nu l} \qquad \text{(VII)}$$

where l is the infrared path length. Typical spectra are shown in Figure 3. The quality of the spectra is typical for the low concentrations used in the environmental chamber experiments. Below we discuss the methods of analysis used to extract reliable concentrations from these spectra.

Results and Discussion

Comparison with Previous Studies. The single point Q-branch cross sections and integrated cross sections are summarized in Tables 2 and 3. IR absorption cross sections from the literature are included for comparison. All values are reported here as base 10 (i.e. $\sigma Cl = \log_{10}(I_0/I)$, which is standard for most FTIR spectrometers). We have given both absolute and effective cross sections. In the latter, the assumption is made that a particular absorbance is due to all the HONO in the sample, rather than just the *trans* or *cis* isomer. This reflects the way that most measurements are actually made, because it is difficult to independently determine the concentrations of the *trans* and *cis* isomers. The absolute cross sections of the *trans* and *cis* isomers are then determined based on the equilibrium

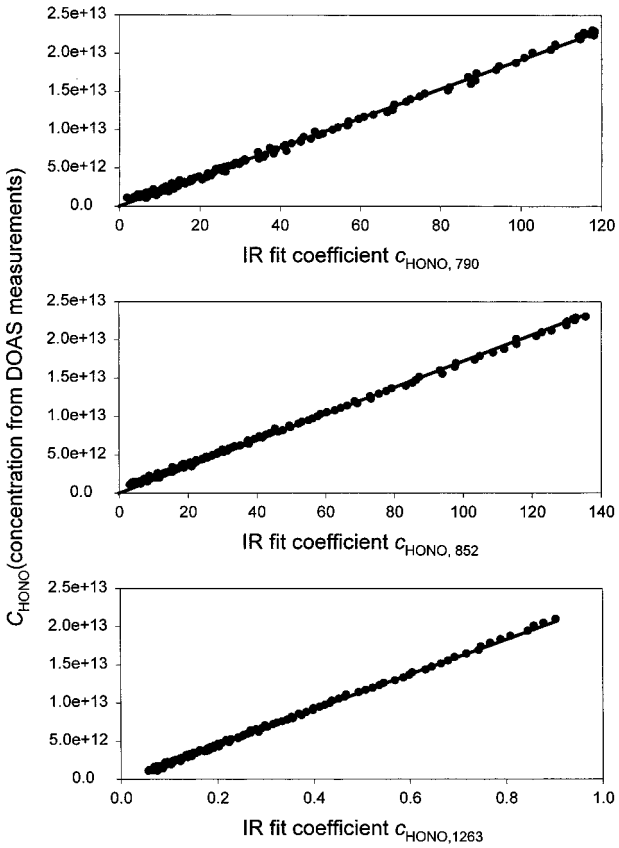

Figure 2. Linear regression fits of uncalibrated concentrations (from IR spectra) to absolute concentrations (from DOAS spectra). Data from experiment 6.

ratio R, defined as $R = [trans]/[cis]$, which is temperature-dependent and is, unfortunately, not firmly established.[37] Previous studies have used different values of R and when converting the published values for comparison to our own, we have used the value of the ratio quoted in the actual study. The following relations were used:

$$\sigma^{eff}_{cis} = \sigma_{cis}\left(\frac{1}{1+R}\right) \qquad \sigma^{eff}_{trans} = \sigma_{trans}\left(\frac{R}{1+R}\right) \qquad \text{(VIII)}$$

In calculating absolute cross sections from our own results, we have used $R = 2.3$, calculated from data given in the JANAF thermochemical tables.[46]

As seen in Table 2, our results are 25−30% lower than those of Chan et al.[29] These authors measured the concentrations of NO, NO_2, and H_2O in their reactor and calculated the partial pressure of HONO using the best known estimate of the equilibrium constant for reactions (2, −2):

$$NO + NO_2 + H_2O \leftrightarrow 2HONO \qquad \text{(2,-2)}$$

HONO and the other oxides of nitrogen are also involved in other equilibria as well,[2,7] e.g., reactions (3,−3):

$$2NO_2 + H_2O \leftrightarrow HONO + HNO_3 \qquad \text{(3,-3)}$$

Becker et al.[34] noted that other tunable diode laser line-strength measurements, in which HONO concentrations were calculated by the equilibrium method, differed from each other by as much as a factor of 3.

Sakamaki et al.[8] determined cross sections of HONO in their fluoropolymer-coated environmental chamber using a chemiluminescence NO_y analyzer as described by Cox.[47] This

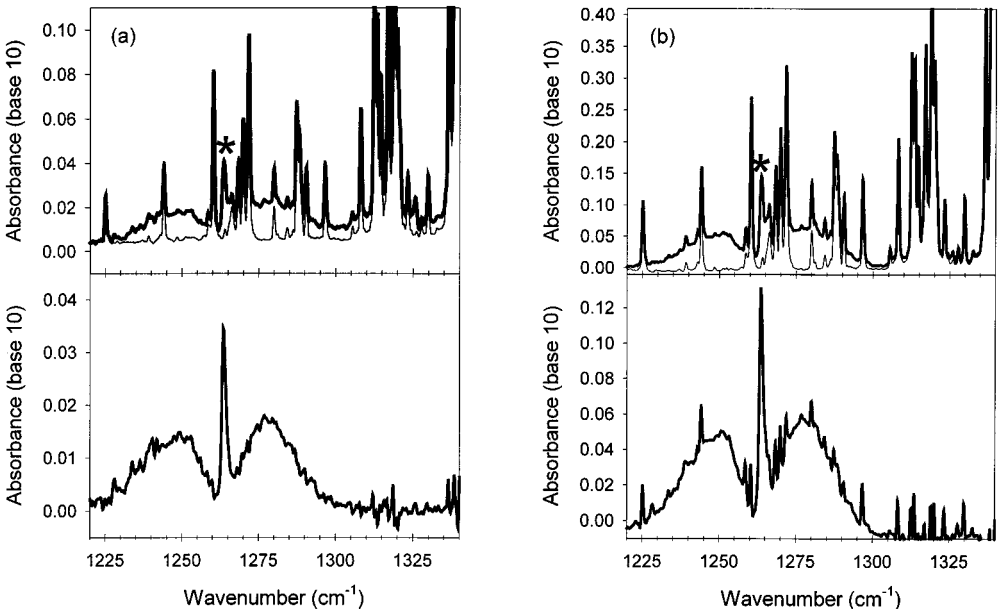

Figure 3. Example of water subtraction from IR spectra. In upper plots, asterisk (∗) indicates position of HONO Q-branch. (a) Low water vapor concentration; subtraction works very well. (b) Higher water vapor concentration; some residual water lines remain in spectrum. In both of these cases the HONO absorption at the Q-branch is large relative to the water absorption, so the Q-branch intensity remains fairly accurate. The thin line is the water reference spectrum in each case.

TABLE 2: Infrared Absorption Cross Sections: Q-Branch Intensity at Given Wavenumber

	effective[a] cross section σ (10^{-19} cm^2 molecule^{-1}, base 10)				absolute[b] cross section σ (10^{-19} cm^2 molecule^{-1}, base 10)			
	790 cm^{-1}	852 cm^{-1}	1263 cm^{-1}	*trans*/*cis* ratio used	790 cm^{-1}	852 cm^{-1}	1263 cm^{-1}	Q_{1263}/Q_{852}
this work[c]	1.92 ± 0.19	2.72 ± 0.27	3.64 ± 0.36	2.30	2.8 ± 0.28	9.0 ± 0.9	5.22 ± 0.52	0.58
Chan et al.[29]		3.79 ± 0.38	4.82 ± 0.48	2.29		12.5 ± 1.3	6.93 ± 0.70	0.56
Sakamaki et al.[8]		2.86	2.78	2.27		9.34	4.00	0.43

[a] Calculated from $\sigma = (1/lC_{HONO})\log_{10}(I_0/I)$, where C_{HONO} is the total HONO concentration (*trans* plus *cis*). [b] Corrected for the *trans*/*cis* ratio. [c] Error bars are 1 standard deviation. Those of Chan et al.[29] are not stated, and Sakamaki et al.[8] do not give error bars for their cross sections.

TABLE 3: Infrared Absorption Cross Sections: Integrated Band

	integrated effective[a] cross sections S (10^{-18} cm molecule^{-1} base 10)				integrated base 10 absolute[b] cross sections S (10^{-18} cm molecule^{-1} base 10)		
	740−820 cm^{-1}	820−900 cm^{-1}	1220−1300 cm^{-1}	*trans*/*cis* ratio used	740−820 cm^{-1}	820−900 cm^{-1}	1220−1300 cm^{-1}
this work	2.4 ± 0.2	4.4 ± 0.4	7.2 ± 0.7	2.30	6.3 ± 0.6	15 ± 1.5	10 ± 1.0
Kagann and Maki[30]			8.1 ± 1.0	2.0			12.2 ± 1.5

[a] Calculated from $S = (1/lC_{HONO})\int_{band} \log_{10}(I_0(\bar{\nu})/I(\bar{\nu}))\, d\bar{\nu}$, where C_{HONO} is the total HONO concentration (*trans* plus *cis*). [b] Corrected for the *trans*/*cis* ratio.

instrument measures either NO or total NO_y (defined as NO + NO_2 + HONO + HNO_3 + N_2O_3 + PAN + organic nitrates + ...) in a gas sample. A scrubber, consisting of a trap containing a 0.1 N aqueous solution of NaOH, was placed in-line before the NO_y analyzer. The trap was intended to remove HONO while leaving NO and NO_2 in the gas stream. Measurements were taken with the scrubber in-line and with the scrubber bypassed, and the difference in total NO_y was taken to be due to HONO. This technique had the disadvantage that some NO and NO_2 are taken up in the trap, with uptake fractions of approximately 20% and 40%, respectively, reported by Sakamaki et al.[8] for their system. This was given by the authors as the primary source of uncertainty in their experiment.

As shown in Table 2, our value for the *cis*-ν_4 cross section maximum at 852 cm^{-1} is in excellent agreement with that of Sakamaki et al.;[8] however, our value for the *trans*-ν_3 maximum is 33% larger. As seen from the ratio Q_{1263}/Q_{852}, this reflects a difference in the relative intensity of the two Q-branches, so it cannot be attributed to error in measuring HONO concentrations. However, our measured ratio of the Q-branch cross sections is in very good agreement with that of Chan et al.[29] One cause of such a discrepancy might be a difference in the actual *trans*/*cis* ratio present during the experiments; the studies of Sakamaki et al.[8] were done at 30 °C, while ours and those of Chan et al.[29] were carried out at 23 °C. However, the calculated[46] *trans*/*cis* ratio changes by only 2% over this temperature range, so it cannot explain the large observed difference in the Q-branch ratios. It is more likely that these ratios are affected by differences in subtraction of water from the spectra.

Water Subtraction. Water has a large effect on determination of HONO Q-branch cross sections, because water absorptions underlie the Q-branches at both 852 and 1263 cm^{-1}. Water subtraction is especially difficult because, at high partial pressures, water absorption is not linear with respect to concentration and subtraction of large peaks tends to produce noisier spectra.[48] We have found it is possible to subtract water relatively well by using a reference spectrum taken at very nearly the same partial pressure of water that was present during the

TABLE 4: Absorbance Ratios of HONO to Water for Q-Branches of Some Typical Spectra[a]

	852 cm^{-1}			1263 cm^{-1}			
[H_2O] (10^{17} molecules cm^{-3})	A_{HONO} (10^{-3} abs units)	A_{H_2O} (10^{-3} abs units)	A_{HONO}/A_{H_2O}	A_{HONO} (10^{-3} abs units)	A_{H_2O} (10^{-3} abs units)	A_{HONO}/A_{H_2O}	Q_{1263}/Q_{852}
1.6	100	11	9.1	130	5.1	25	0.56
0.39	25	1.3	19	35.	7.2	4.9	0.61
0.72	23	9.3	2.5	21	7.9	2.7	0.40

[a] $Q_{1263}/Q_{852} = (1/R)(A_{HONO}(1263)/A_{HONO}(852))$, where the *trans*/*cis* ratio $R = 2.30$.

experiment. Figure 3a shows the region around the 1263 cm^{-1} band before and after subtraction of water; the water vapor concentration in this case was approximately 4×10^{16} molecules cm^{-3}, about 1000 times the HONO concentration. At higher water concentrations, subtraction becomes more difficult, and the resultant spectrum may contain residual water lines, as shown in Figure 3b, where [H_2O] $\approx 1.5 \times 10^{17}$ molecules cm^{-3}. The effect of these lines can be determined by examining the Q-branch absorbance ratio Q_{1263}/Q_{852}. The different water lines underlying these two Q-branches make this ratio very sensitive to water interference.

Table 4 shows the absorbance of HONO and of water (A_{HONO} and A_{H_2O}, respectively) and the absorbance ratio of HONO to water at 1263 and 852 cm^{-1} for some typical spectra where the water vapor concentration varies from $(0.39-1.6) \times 10^{17}$ molecules cm^{-3}. If A_{HONO}/A_{H_2O} is large, small errors in water subtraction will make little difference in the ratio Q_{1263}/Q_{852}. This is the case for the first two spectra listed, where the water absorbance at either Q-branch is no more than ~20% of the HONO absorbance. In the third case listed, the water peak is approximately 40% as large as the HONO absorbance, and for this case a significant difference in Q_{1263}/Q_{852} is seen. This difference in Q-branch ratios is of similar magnitude to that described above between our results and those of Sakamaki et al.,[8] and provides a likely explanation for the discrepancy.

High-Resolution Studies. Kagann and Maki[30] measured the spectra of equilibrium mixtures of NO, NO_2, and H_2O. They calculated the concentration of HONO based on the equilibrium of reaction 2,−2 as well as several other equilibria in which N_2O_3, N_2O_4, and HNO_3 are formed, but apparently not reaction 3,−3. Their results cannot be compared to those of Sakamaki et al.[8] and Chan et al.[29] because they did not report Q-branch maxima. However, our integrated base 10 band intensity of $(7.2 \pm 0.7) \times 10^{-18}$ cm molecule^{-1} for the *trans*-ν_3 band at 1263 cm^{-1} is in good agreement with their reported value of $(8.1 \pm 1.0) \times 10^{-18}$ cm molecule^{-1} (see Table 3).

Becker et al.[34] have published TDLS line intensities, but we cannot compare these to our results, because their reported high-resolution lines cover only a small part of the P branch near 1255 cm^{-1}. To our knowledge, theirs is the only TDLS study in which line intensities were reported.

Model References. Least-squares fitting using reference spectra is often preferable to integration or Q-branch measurements because it is not as strongly dependent on the location of the baseline or on the intensity of any one peak; it can therefore extend the effective sensitivity of IR measurements to much lower concentrations. There are advantages to more traditional methods, however: Q-branch intensities are very useful for quickly estimating concentrations, and band integrations are resolution-independent. For this reason, we have reported in Tables 2 and 3 both the results of a fit approach as well as the Q-branch cross sections and the integrated absorbances.

Figure 4 shows our measured reference spectra for the *trans*-ν_3 band at 1263 cm^{-1} and *cis*-ν_4 band at 852 cm^{-1} as well as

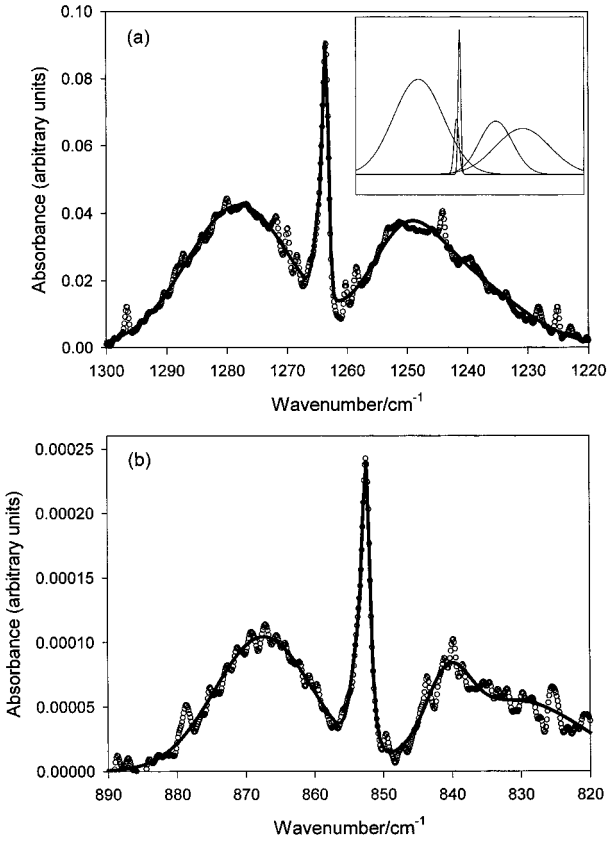

Figure 4. (a) Actual *trans*-ν_3 reference spectrum (circles) compared to 5-Gaussian model spectrum (solid line). Inset shows the five Gaussian functions used. (b) The actual and model *cis*-ν_4 references. Spectra were recorded at 0.5 cm^{-1} resolution with 1 level of zero filling.

simulated spectra using a sum of Gaussian functions:

$$S(\bar{\nu}) = \sum_{m=1}^{M} \alpha_m e^{-\beta_m(\bar{\nu}-\gamma_m)2} \qquad \text{(IX)}$$

The choice of Gaussian functions was based on similarity to the experimental spectra, but does not have any physical significance. The parameters α_m, β_m, and γ_m determine the intensity, width, and position, respectively, of the *m*th Gaussian function. The smallest number of functions which gave a good fit to the data was $M = 5$. The optimum values of the parameters, given in Table 5, were determined by least-squares fitting.

Figure 5 compares the HONO concentration−time profiles for a typical experiment (no. 5) using in one case the measured HONO spectra, and in the other case the simulated spectra determined by the Gaussian fit approach. The agreement between the two is excellent, differing by less than 5% in all cases.

Uncertainty, Detection Limit, and Linearity. A conservative estimate of our uncertainties was calculated by propagating the errors in the regression (VI) and the spectral fit (V), as well

TABLE 5: Parameters Used To Generate Model Reference Spectra[a]

	852 cm^{-1}			1263 cm^{-1}		
m	α_m (10^{-19} cm^2 $molecule^{-1}$)	β_m (cm^2)	γ_m (cm^{-1})	α_m (10^{-19} cm^2 $molecule^{-1}$)	β_m (cm^2)	γ_m (cm^{-1})
1	1.19 ± 0.05[b]	0.0098 ± 0.0002	867.38 ± 0.08	1.73 ± 0.03	0.0065 ± 0.0001	1277.9 ± 0.1
2	0.577 ± 0.003	0.051 ± 0.006	840.6 ± 0.1	0.98 ± 0.09	0.015 ± 0.003	1250.8 ± 0.2
3	1.64 ± 0.07	2.1 ± 0.2	852.37 ± 0.02	1.0 ± 0.3	0.69 ± 0.26	1264.6 ± 0.3
4	0.622 ± 0.004	0.0054 ± 0.0005	830.7 ± 0.5	0.82 ± 0.05	0.0055 ± 0.0015	1241.4 ± 3.4
5	1.01 ± 0.05	0.31 ± 0.02	853.12 ± 0.07	2.6 ± 0.9	2.3 ± 0.3	1263.52 ± 0.02

[a] These parameters are used in conjunction with eq IX to produce model references. References can be used to analyze spectra with MFC[42] or with any other software which can perform a linear least-squares fit between two sets of data. [b] Error bars are 1 standard deviation and reflect only the uncertainty associated with the nonlinear fit. See Table 2 for the error bars of the actual measured cross sections.

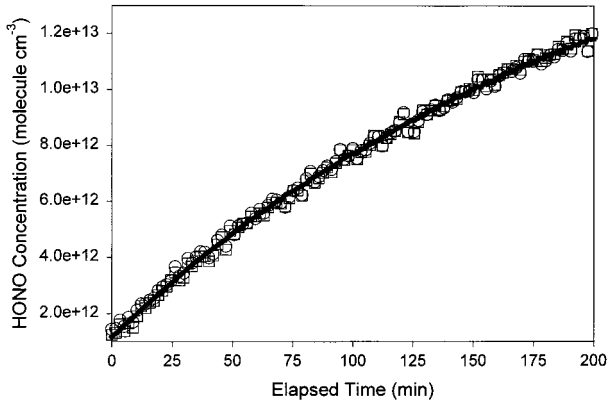

Figure 5. Comparison of HONO concentrations for experiment no. 5 determined from actual (squares) 1263 cm^{-1} reference spectra to simulated reference spectra (circles). The concentrations determined by DOAS are shown as a heavy line. Data for the 852 cm^{-1} peak are similar.

as errors due to water subtraction and to the uncertainty in the DOAS measurements and in the IR and UV path length. Our conclusion is that the limiting source of error in our experiments is the signal-to-noise ratio of our IR HONO spectra, which is on the order of about 10% for each band. This gives the 1σ error bars quoted in Tables 2 and 3. We used different HONO sources ($ClNO + H_2O$ and $HCl + NaNO_2$) to reduce the possibility of systematic error relating to impurities, and Table 1 shows that our reproducibility for a_ν between the two types of experiments was about 5%, consistent with our error estimate. The errors associated with the maximum UV cross sections of Bongartz et al., from their Table 2, range from 0.9 to 1.8% (1σ), so these do not contribute very significantly to our error. Although some recent measurements (e.g., Pagsberg et al.[49]) give slightly different values, the Bongartz et al. cross sections are in good agreement with a very recent measurement by Stutz et al.[50] in which very high-purity (almost NO_2-free) samples of HONO were used.

Our IR detection limit at 52.53 m is between 50 and 80 ppb, and the IR measurements are in very good ($\leq$10%) agreement with the DOAS measurements for HONO concentrations of 75 ppb and higher. Figure 2 shows the absorbance to be linear in the absorbance regimes used in our experiments. This linearity was found to hold up to the highest concentration−path length product used in these experiments (3.4 ppm at 52.53 m path length).

Conclusions

New measurements of HONO absorption cross sections for three bands in the infrared have been made. Unlike previous studies in which the HONO concentrations were determined indirectly, we have measured HONO directly by UV/visible (DOAS) spectroscopy. In the event of a future correction to the DOAS cross sections on which the IR cross sections are based, our values can easily be adjusted accordingly.

We have given synthetic reference spectra for the 852 and 1263 cm^{-1} bands that can be easily reproduced by any computer program capable of calculating a Gaussian function. These references give nearly identical results when used for spectral analysis in place of our actual reference spectra. We hope that this will facilitate the use of least-squares fitting in analysis of HONO spectra, which we have found to be a much more reliable technique than either integration or measurement of Q-branch intensities. While these measurements have been made at room temperature, clearly additional studies as a function of temperature, particularly to lower temperatures, would be useful for atmospheric applications.

Acknowledgment. We gratefully acknowledge M. Ezell and N. Saliba for experimental assistance, W. P. L. Carter, T. Wallington, and M. Hurley for helpful discussions, L. Moritz and J. Meyer for equipment fabrication, and the California Air Resources Board (Contract No. 97-311) for financial support.

References and Notes

(1) Winer, A. M.; Biermann, H. W. *Res. Chem. Intermed.* **1994**, *20*, 423.

(2) Finlayson Pitts, B. J.; Pitts, J. N., Jr. *Chemistry of the Upper and Lower Atmosphere*; Academic Press: San Diego, CA, 2000.

(3) Kleffmann, J.; Becker, K. H.; Wiesen, P. *Atmos. Environ.* **1998**, *32*, 2721.

(4) Wiesen, P.; Kleffmann, J.; Kurtenbach, R.; Becker, K. H. *Faraday Discuss.* **1995**, *100*, 121.

(5) Khalil, M. A. K.; Rasmussen, R. A. *J. Geophys. Res.* **1992**, *97*, 14651.

(6) Prather, M.; Derwent, R.; Ehhalt, D.; Fraser, P.; Sanhueza, E.; Zhou, X. In *Climate Change 1995, The Science of Climate Change, Contribution of Working Group I to the Second Assessment Report of the Intergovernmental Panel on Climate Change*; Houghton, J. T., Meira Filho, L. G., Callander, B. A., Harris, N., Kattenberg, A., Maskell, K., Eds.; Cambridge University Press: New York, 1996; Chapter 2.

(7) Lammell, G.; Cape, J. N. *Chem. Soc. Rev.* **1996,** *25*, 361, and references therein.

(8) Sakamaki, F.; Hatakeyama, S.; Akimoto, H. *Int. J. Chem. Kinet.* **1983**, *15*, 1013.

(9) Pitts, J. N., Jr.; Sanhueza, S.; Atkinson, R.; Carter, W. P.; Winer, A. M.; Harris, G. W.; Plum, C. N. *Int. J. Chem. Kinet.* **1984**, *16*, 919.

(10) Akimoto, H.; Takagi, H.; Sakamaki, F. *Int. J. Chem. Kinet.* **1987,** *19*, 539.

(11) Jenkin, M. E.; Cox, R. A.; Williams, D. J. *Atmos. Environ.* **1988**, *22*, 487.

(12) Svenssen, R.; Ljungström, E.; Lindqvist, O. *Atmos. Environ.* **1987**, *21*, 1529.

(13) Febo, A.; Perrino, C. *Atmos. Environ.* **1991**, *25A*, 1055.

(14) Bambauer, A.; Branter, B.; Paige, M.; Novakov, T. *Atmos. Environ.* **1994**, *28*, 3225.

(15) Mertes, S.; Wahner, A. *J. Phys. Chem.* **1995**, *99*, 14000.

(16) Goodman, A. L.; Underwood, G. M.; Grassian, V. H. *J. Phys. Chem. A* **1999,** *103*, 7217.

(17) Barney, W. S.; Finlayson-Pitts, B. J. *J. Chem. Phys. A* **2000**, *104*, 171.

(18) Pitts, J. N., Jr.; Wallington, T. J.; Biermann, H. W.; Winer, A. M. *Atmos. Environ.* **1985,** *19*, 763.
(19) Spicer, C. W.; Kenny, D. V.; Ward, G. F.; Billick, I. H. *J. Air Waste Manage. Assoc.* **1993**, *43*, 1479.
(20) Brauer, M.; Ryan, P. B.; Suh, H. H.; Koutrakis, P.; Spengler, J. D.; Leslie, N. P.; Billick, I. H. *Environ. Sci. Technol.* **1990**, *24*, 1521.
(21) Ammann, M.; Kalberer, M.; Jost, D. T.; Tobler, L.; Rössler, E.; Piguet, D.; Gäggeler, H. W.; Baltensperger, U. *Nature* **1998**, *395*, 157.
(22) Gerecke, A.; Thielmann, A.; Gutzwiller, L.; Rossi, M. J. *Geophys. Res. Lett.* **1998**, *25*, 2453.
(23) Longfellow, C. A.; Ravishankara, A. R.; Hanson, D. R. *J. Geophys. Res.* **1999,** *104*, 13833.
(24) Kalberer, M.; Ammann, M.; Arens, F.; Gäggeler, H. W.; Baltensperger, U. *J. Geophys. Res.* **1999**, *104*, 13825.
(25) Perner, D.; Platt, U. *Geophys. Res. Lett.* **1979**, *6*, 917.
(26) Karlsson, R. S.; Ljungström, E. B. *Environ. Sci. Technol.* **1996**, *30*, 2008.
(27) Wallington, T. J.; Japar, S. M. *J. Atmos. Chem.* **1989,** *9*, 399.
(28) Junkermann, W.; Ibusuki, T. *Atmos. Environ.* **1992,** *26A*, 3099.
(29) Chan, W. H.; Nordstrom, R. J.; Calvert, J. G.; Shaw, J. H. *Environ. Sci. Technol.* **1976,** *10*, 674.
(30) Kagann, R. H.; Maki, A. G. *J. Quant. Spectrosc. Radiat. Transfer* **1983,** *30*, 37.
(31) Vogt, R.; Finlayson-Pitts, B. J. *Geophys. Res. Lett.* **1994**, *21*, 2291.
(32) Wingen, L. M.; Barney, W. S.; Lakin, M. J.; Brauers, T.; Finlayson-Pitts, B. J.; *J. Phys. Chem. A* **2000**, *104*, 329.
(33) Maki, A. G. *J. Mol. Spectrosc.* **1988,** *127*, 104.
(34) Becker, K. H.; Kleffmann, J.; Kurtenbach, R.; Wiesen, P.; Febo, A.; Gherardi, M.; Sparapani, R. *Geophys. Res. Lett.* **1995,** *22*, 2485, and references therein.
(35) Febo, A.; Perrino, C.; Gherardi, M.; Sparapani, R. *Environ. Sci. Technol.* **1995**, *29*, 2390.
(36) Bongartz, A.; Kames, J.; Schurath, U.; George, Ch.; Mirabel, Ph.; Ponche, J. L. *J. Atmos. Chem.* **1994**, *18*, 149.
(37) Bongartz, A.; Kames, J.; Welter, F.; Schurath, U. *J. Phys. Chem.* **1991**, *95*, 1076.
(38) De Haan, D. O.; Brauers, T.; Oum, K.; Stutz, J.; Nordmeyer, T.; Finlayson-Pitts, B. J. *Int. Rev. Phys. Chem.* **1999**, *18*, 343.
(39) White, J. U. *J. Opt. Soc. Am.* **1942**, *32*, 285.
(40) De More, W. B.; Sander, S. P.; Golden, D. M.; Hampson, R. F.; Kurylo, M. J.; Howard, C. J.; Ravishankara, A. R.; Kolb, C. E.; Molina, M. J. *Chemical Kinetics and Photochemical Data for Use in Stratospheric Modeling*; JPL Publication 97-4; NASA/JPL: Pasadena CA, 1997.
(41) Hjorth, J.; Ottobrini, G.; Cappellani, F.; Restelli, G. *J. Phys. Chem.* **1987,** *91*, 1565.
(42) Gomer, T.; Brauers, T.; Heintz, T.; Stutz, J.; Platt, U. MFC Version 1.98, 1995.
(43) Platt, U.; Hausmann, M. *Res. Chem. Intermed.* **1994,** *20*, 557.
(44) Stutz, J.; Platt, U. *Appl. Opt.* **1996,** *30*, 6041−6053.
(45) Davidson, J. A.; Cantrell, C. A.; McDaniel, A. H.; Shetter, R. E.; Madronich, S.; Calvert, J. G. *J. Geophys. Res.* **1988**, *93*, 7105.
(46) Chase, M. W. *NIST-JANAF Thermochemical Tables*, 4th ed.; *J. Phys. Chem. Ref. Data* Monograph No. 9; American Institute of Physics: Woodbury, NY, 1998.
(47) Cox, R. A. *J. Photochem.* **1974** *3*, 175.
(48) Weis, D. D.; Ewing, G. *Anal. Chem.* **1998,** *70*, 3175.
(49) Pagsberg, P.; Bjergbakke, E.; Ratajczak, E.; Sillesen, A. *Chem. Phys. Lett.* **1997,** *272*, 383.
(50) Stutz, J.; Kim, E. S.; Platt, U.; Bruno, P.; Perrino, C.; Febo, A. *J. Geophys. Res.*, submitted for publication.